A unified figure of merit for interband and intersubband cascade devices

Wenxiang Huang[1,2] *, S.M. Shazzad Rassel[1], Lu Li[1], Jeremy A. Massengale[1,2], Rui Q. Yang[1] *, Tetsuya D. Mishima[2], and Michael B. Santos[2]

[1]School of Electrical and Computer Engineering, University of Oklahoma, Norman, Oklahoma 73019, USA

[2]Homer L. Dodge Department of Physics and Astronomy, University of Oklahoma, Norman, Oklahoma 73019, USA

*wxhuang@ou.edu; Rui.q.Yang@ou.edu

Abstract

By exploring a semi-empirical model, the saturation current density J_0 is identified to manifest the significant difference in carrier lifetime between interband cascade devices (ICDs) and intersubband quantum cascade devices (QCDs). Based on this model, the values of J_0 have been extracted for a large number of ICDs and QCDs from their current-voltage characteristics at room temperature. By analyzing and comparing available ICD and QCD data, we demonstrate how J_0 can be used as a unified figure of merit to evaluate both interband and intersubband cascade configurations for their device functionality. The significance of J_0 on the performances of mid-infrared detectors and photovoltaic cells is illustrated by comparing the measured detectivity (D^*) and the estimated open-circuit voltage (V_{oc}), respectively. From extracted values of J_0, which are more than one order of magnitude lower in ICDs than that in QCDs with similar transition energies in active regions, and discussion of the consequences on device performance, the advantages of interband cascade configurations over intersubband quantum cascade configurations have been clearly revealed based on the same framework. The overall picture for both QCDs and ICDs sheds light from the perspective of a united figure of merit, which will provide useful guidance and stimulation to the future development of both ICDs and QCDs.

Keywords: Interband cascade, quantum cascade, saturation current density, open-circuit voltage

1. Introduction

Mid-infrared (IR) devices are needed to meet the growing demands of many applications such as gas sensing (from environmental and chemical-warfare monitoring to detection of pipe leaks and explosives), infrared countermeasures (IRCM), IR lidar, thermal imaging, medical diagnostics, free-space communications, thermophotovoltaic (TPV) cells, and IR illumination. In the IR spectrum, two major families of semiconductor optoelectronic devices operate with cascade configurations. Quantum cascade (QC) devices are based on intersubband transitions within the same band (*e.g*. the conduction band), while interband cascade (IC) devices are based on interband transitions between the conduction and valence bands. The family of IC devices (ICDs) includes IC lasers [1-4], IC infrared photodetectors (ICIPs) [5-6], and IC photovoltaic (ICPV) cells [7-8]. QC devices (QCDs) include QC lasers [9-11] and QC detectors [12-13]. Although QC structures were also proposed and simulated theoretically [14-15] for PV cells, none have been reported experimentally. Both IC and QC devices are based on quantum-engineered layer structures, and have been developed nearly in parallel with remarkable advances, especially in lasers [2-4, 9-11]. However, they were frequently discussed and presented without reference to their counterparts. In particular, there has been no evaluation or comparison based on a common figure of merit to fairly describe their characteristics with different device functionalities. Fundamentally, ICDs and QCDs are very different in terms of activated processes and distinct carrier lifetimes, *i.e.* picosecond range for fast phonon scattering in QCDs vs. nanosecond range for Auger and Shockley-Read-Hall (SRH) recombinations in ICDs. However, this difference in carrier lifetime and their current-voltage characteristics can be described by a single equation based on a semi-empirical model. In this work, such a model is employed to extract the saturation current density J_0 from many QCDs and ICDs reported in the literature [13, 16-25] and some of our unpublished ICDs. It is shown in this letter that J_0 is closely connected to the carrier lifetime and can be considered as a unified figure of merit for both QC and IC families of devices to reflect their device characteristics and performance.

Based on more than 20 years of studies on QC lasers (QCLs) and IC lasers (ICLs), it is well known that the relatively much longer carrier lifetime in ICDs has resulted in a significantly lower threshold current density (J_{th}) and power consumption at the threshold in ICLs at room temperature compared to that in QCLs. This has been demonstrated for a wide IR spectral region (2.7-6 μm) [3-4]. The reverse bias characteristic data for extracting J_0 are not readily available for QCLs as they usually operate under forward bias. Hence, our analysis of QCDs mainly focuses on room temperature (RT) QC detectors reported in the literature [13, 16-20]. Some ICDs included in our study are IC laser structures that were reported previously [21-25], while the others were designed as IC light emitting devices (LEDs). Except one device based on type-I quantum well active region [23], the active regions of these ICDs are made of an asymmetric "W" quantum well (QW) [26] that comprises two InAs electron QW layers on both sides of the GaInSb hole QW layer. The number of cascade stages (N_c) for these ICDs is between 6 to 15. ICDs composed of InAs/Ga(In)Sb type-II superlattices (SLs) studied in [27-34] are also included due to their detector and PV performances and denoted by "ICD_SL" to differentiate from those having QWs in their active regions. Most of these ICDs are square mesa type devices along with several broad area IC lasers.

2. Semi-empirical Model for Dark Current Density

Since the electronic states near the two ends of each cascade stage are located in a low energy level on one end and a high energy level on the other, a potential barrier region is formed between these two ends. When a forward bias (positive on the high energy end) is applied to a cascade stage, the number of available carriers that can overcome the potential barrier to move from the low energy end to the high energy end is increased exponentially with the bias voltage and, consequently, so is the forward current density; while the reverse current density approaches a constant (J_0) value because the number of carriers that can move from the high energy end does not increase with the reverse bias voltage. Hence, in a semi-empirical model, the current density (J_d) - voltage (V) characteristics in a cascade device with identical cascade stages can be described by:

$$J_d = J_0(e^{qV/N_c k_b T} - 1) \tag{1}$$

where q is electron charge, k_b is the Boltzmann constant, and T is temperature. Qualitatively, this is similar to the diode equation for a *p-n* junction. Eq. (1) can be derived from a fundamental level with lengthy mathematical manipulations, which were discussed in detail in Ref. 35 for ICDs and in Refs. 36-38 for QCDs. Here, our approach captures a major feature in cascade devices and provides a simple way to derive Eq. (1) for current-voltage characteristics in complicated cascade structures, revealing an instructive connection with *p-n* junctions. This has not been reported previously in the literature and should be beneficial in helping promote a better understanding of complex cascade devices. It has been shown that J_0 is proportional to the carrier concentration and inversely proportional to the carrier lifetime due to various scattering mechanisms such as defects, doping, phonons and Auger recombination. This relationship has been explored by us to obtain the carrier lifetime for ICIPs [39]. From Eq. (1), the product of device zero-bias resistance R_0 and area A can be obtained as:

$$R_0 A = \frac{N_c k_b T}{q J_0} \tag{2}$$

and is an important parameter for evaluating detector performance.

In principle, the value of J_0 for ICDs and QCDs can be extracted by fitting the J_d-V curves to Eq. (1). However, in a real device, shunt and series resistances (R_{shunt} and R_s) are often present. Considering these factors, the J_d-V curve can be fitted to a modified equation:

$$J_d = J_0(e^{q(V - R_s A J_d)/N_c k_b T} - 1) + \frac{V - R_s A J_d}{R_{shunt} A} \tag{3}$$

where A is the device area.

3. Saturation Current Density for Cascade Devices

According to Eq. (3), the three parameters, J_0, R_{shunt} and R_s, can be extracted by using the least-square fitting method. For the fits, the values of R_{shunt} and R_s were kept in the range of 10^3-10^4 and 1-10 Ω, respectively. As an example, the measured J_d-V curves and fitting results for a large area (400 μm×400 μm) eight-stage ICD (wafer R083 in Ref. 22) and a fifty-stage QCD (110 μm×110 μm) [20] at 300 K are shown in Fig. 1. The two devices have the same transition energy ΔE of 0.23 eV in the active region at 300 K, which is the bandgap for the ICD or the energy separation of the two involved conduction subbands for the QCD. As can be seen in Fig. 1, J_d is at least an order of magnitude lower in the ICD than in the QCD. This difference is attributed to having comparatively much longer carrier lifetimes in the ICD. We found that Eq. (3) provides an excellent fit with the measurements, supporting the validity of the semi-empirical model used in this work. Specifically, the extracted J_0 (R_{shunt}) based on Eq. (3) is 0.017 A/cm^2 (5945 Ω) and 1.8 A/cm^2 (6772 Ω) for the eight-stage ICD and fifty-stage QCD, respectively. The other fitting parameter R_s is 5 Ω for the ICD, and 7 Ω for the QCD with a smaller device area.

Based on the model with fits to Eq. (3), the extracted values of J_0 are plotted in Fig. 2 for a number of ICDs [21-25] and QCDs [13, 16-20] at 300 K. As shown in Fig. 2, the value of J_0 is more than one order of magnitude lower in ICDs than in QCDs with similar ΔE, showing the significant effect of carrier lifetime on transport current, which is consistent with the threshold behavior in laser performance for a wide infrared spectral region mentioned earlier. It is evident in Fig. 2 that J_0 tends to increase exponentially with a decrease in ΔE (or inverse wavelength $1/\lambda = \Delta E/hc$ where h is Planck's constant and c is the speed of light) for both ICDs and QCDs. This is because the thermally generated carrier concentration is inversely proportional to an exponential function of ΔE. It should be pointed out that ICDs are more sensitive to surface leakage currents because of the presence of surface states in their bandgap. Hence the extracted J_0 in Fig. 2 might be more overestimated for ICDs than for QCDs. Because of the substantial variation in device area, the product of the resistance and area is a more appropriate quantity as used effectively in Eq. (3). Generally, the value of $R_{shunt}A$ extracted from fitting is smaller for QCDs compared to ICDs. However, the ratio of $R_{shunt}A$ to R_0A is typically higher in QCDs than in ICDs, which reflects the relatively lower percentage of surface leakage in QCDs than in ICDs. Moreover, material qualities and processing technologies between different groups may differ substantially. Overall, the extracted values of J_0 are much lower in ICDs than in QCDs, which not only manifests significantly different threshold current densities and power consumption in lasers between the two families, but also results in considerable differences in detector and PV device performance as discussed in next two sections. The very significant difference in J_0 between ICDs and QCDs is fundamentally attributed to their distinctive carrier lifetimes as J_0 is inversely proportional to the lifetime. In QCDs, longitudinal optical (LO) phonon scattering is dominant and fast (in ps or shorter) between and within the conduction subbands of the QWs. In ICDs and at high temperatures, Auger and SRH (through defects) processes are the main scattering mechanisms. With interband transitions, the carrier lifetime is in the nanosecond range and is three orders of magnitude longer than for phonon scattering. The extracted J_0 is much lower in ICDs compared to in QCDs, which unambiguously confirms the much longer lifetime in ICDs (~ns) than in QCDs (~ps).

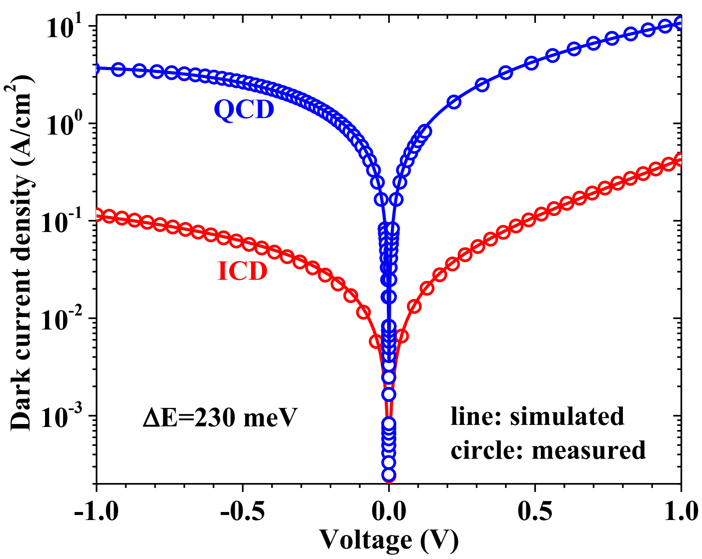

Fig. 1. The measured and fitted J_d-V curves for a 8-stage ICD and a 50-stage QCD at 300 K. The ICD and QCD were mentioned in Ref. 22 (wafer R083) and Ref. 20, respectively.

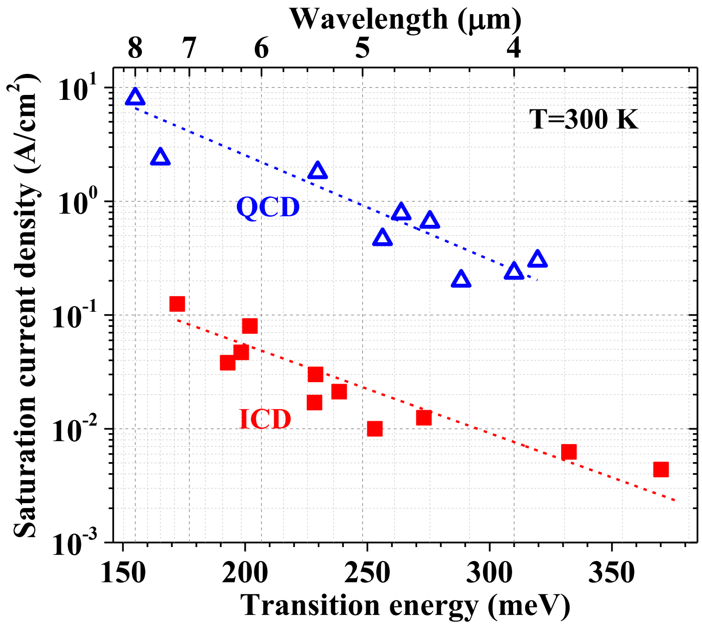

Fig. 2. The extracted values of J_0 for ICDs and QCDs at 300 K. Some ICDs have been described previously in Refs. 21-25, while others are from our unpublished studies. The QCDs are from Refs. 13 and 16-20.

4. Effect of J_0 On the Performances of Detectors

The saturation current density J_0 is a measure of Johnson noise in a photodetector. The R_0A mentioned in Eq. (2) is also reflected in the specific detectivity D^*, which is essentially a measure of signal to noise ratio – a common figure of merit for a photovoltaic photodetector operating at zero bias, and is defined by:

$$D^* = R_i\sqrt{\frac{R_0A}{4k_bT}} \tag{4}$$

where R_i is the responsivity. The measured peak R_i for ICDs and QCDs at 300 K is shown in Fig. 3 (a). In addition to some of the ICDs presented in Fig. 2, another two ICDs (devices A and B in Ref. 5) and ICD_SLs from Refs. 27-34 are included in Figs. 3 (a) and (b). As can be seen in Fig. 3(a), the peak R_i is generally higher in ICDs than in QCDs, and is especially high in ICD_SLs with SL absorbers used for enhancing absorption. The lower R_i in QCDs is partially attributed to the low escape probability p_e that is proportional to the carrier lifetime [13, 40] for QCDs, while this value is close to unity for ICDs with the much longer lifetime [6]. Another reason might be related to the polarization selection rule for intersubband transitions in conduction band QWs [40-41], which prohibits the absorption of normal incidence light in QCDs. To accommodate normal incidence light, QCDs typically have facets made by polishing at an angle of 45° to the growth direction. In addition, an improved responsivity can be achieved for intersubband photodetectors by employing a photonic metamaterial that can enhance the light-matter interaction. This was recently demonstrated in QW IR photodetectors (QWIPs) with photo-conductive gain near 9 μm at RT [42], in which the responsivity (~0.2 A/W) in the QWIP is comparable to those in ICD_SLs as shown in Fig. 3(a). However, due to significant noise with a high dark current density, its detectivity D^* (~2.8×10^7 Jones) is about one order of magnitude lower than that in ICD_SLs with similar ΔE as shown in Fig. 3(b).

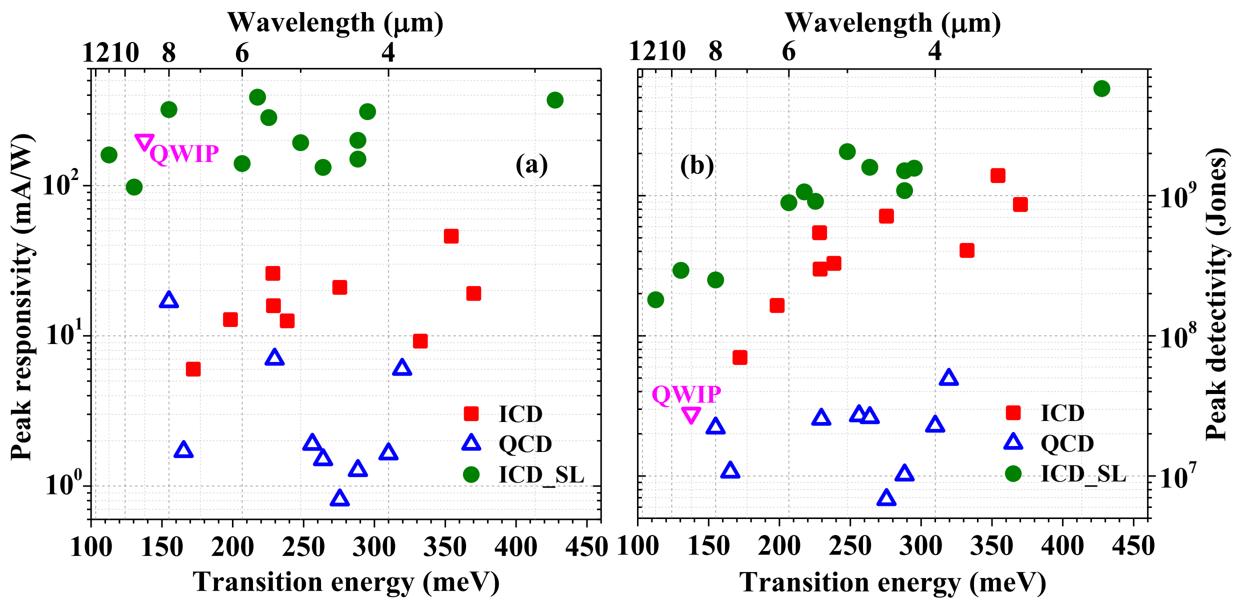

Fig. 3. Measured peak (a) responsivities and (b) detectivities for ICDs, ICD_SLs and QCDs at 300 K. In addition to some of the ICDs presented in Fig. 2, two ICDs (devices A and B in Ref. 5) and all ICD_SLs from Refs. 27-34 are included. One QWIP is from Ref. 42.

According to Eqs. (2) and (4), D^* is inversely proportional to the square root of J_0. The measured peak D^* values at 300 K for the studied ICDs and QCDs are shown in Fig. 3 (b). As can be seen in this figure, the values of D^* are nearly one order of magnitude higher for ICDs than for QCDs. At 300 K, the attainable D^* in most QCDs is less than 3×10^7 Jones due mainly to a high J_0, while most D^* values for ICDs are higher than 1×10^8 Jones and some even exceed 1×10^9 Jones. Also, the difference in D^* between ICDs and QCDs is more significant compared to the difference in R_i between them. This stems from more than one order of magnitude lower J_o in ICDs than in QCDs even though the number of cascade stages N_c (<15) in the ICDs is less than in the QCDs (≥30). If they had the same N_c, the value of D^* would be increasingly larger in ICDs than in QCDs. According to Eqs. (2) and (4), D^* is proportional to the square root of the number of cascade stages if R_i is unchanged. This is approximately correct when individual absorbers are made of a pair QWs or thin, and the total absorber thickness does not cause a substantial attenuation of light intensity [6]. When the light absorption is significant in individual absorbers (*e.g.* especially in ICD_SLs), the attenuation of light intensity along the propagation direction needs to be considered in evaluating the responsivity R_i, which will decrease with an increase in N_c [33,35,43]. In such a scenario, D^* for a non-current matched cascade device (*e.g.* with identical absorbers) will reach a maximum value at a finite N_c as discussed in Refs. 35 and 43. This is particularly true for ICD_SLs where SLs are used in the active region to enhance absorption and responsivity for attaining the highest value of D^* among all devices, as shown in Fig. 3. Nevertheless, compared to ICDs, the additional increase in D^* for ICD_SLs is not as significant as the boost in the peak R_i. This is because J_o is much higher in ICD_SLs with thicker SL absorbers than in ICDs. Nevertheless, with two adjustable parameters, the SL absorber thickness and the number of cascade stages, ICD_SLs can be optimized with more flexibilities to achieve high D^* for better device performance at high temperatures [35,43]. At present, long wavelength (8-12 μm) ICIPs have already been operated at RT and above with D^* exceeding that of commercial uncooled HgCdTe detectors at similar wavelengths [43-44].

Additionally, the voltage responsivity (defined as the ratio of the output signal voltage to the input power) [45] can be used to evaluate the detector performance. Similar to *p-n* diodes, assuming negligible shunt and series resistances, the current density J in ICDs and QCDs under light illumination can be approximately expressed as:

$$J = J_0(e^{qV/N_c k_b T} - 1) - J_{ph} \tag{5}$$

where J_{ph} is the photocurrent, which has been simply presumed to be bias independent. In a real case, the photocurrent may be bias dependent as has been shown in our PV cells based on IC structures [34]. Based on Eq. (5), the open-circuit voltage V_{oc} for an ICD or a QCD is:

$$V_{oc} = \frac{N_c k_b T}{q} \ln\left(\frac{J_{ph}}{J_0} + 1\right) \tag{6}$$

Therefore from Eq. (6), one can see that the lower J_0, the higher V_{oc}, and a high value of J_0 will reduce V_{oc}. Also, when the photocurrent density is smaller than the dark current density, which is common in the detection of weak light at high temperature, V_{oc} can be approximated to first order as:

$$V_{oc} = \frac{N_c k_b T}{q} \frac{J_{ph}}{J_0}, \tag{7}$$

which is linearly proportional to the number of cascade stages and the ratio of photocurrent to saturation current densities. Hence, with the open circuit voltage as the detected signal, more stages and a lower saturation current density will be beneficial for enhanced device performance. According to Fig. 2 and 3, the voltage responsivity will be much higher in ICDs than in QCDs. This is due to the higher photocurrent (proportional to responsivity) and the much lower J_0 in ICDs compared to QCDs. Overall, in terms of either current or voltage responsivity, ICDs will have advantages over QCDs.

5. Effect of J_0 On the Performances of Photovoltaic Cells

Regarding photovoltaic cells to convert light into electricity, the saturation current density J_0 remains an important parameter to evaluate device performance. Since the transition energy ΔE in the active region of ICDs and QCDs is in the mid-infrared region, based on the Shockley-Queisser detailed balance model [46], they are appropriate for a TPV application [47-49] with the heat source temperature typically in the range of 1300-2000 K. Indeed, TPV cells based on IC structures have been experimentally demonstrated with high open-circuit voltage V_{oc} exceeding the single bandgap determined value, showing the cascade effect [8,34,49]. In contrast, TPV cells based on QC structures have not been reported experimentally, possibly due to high values of J_0 in QCDs.

Based on Eq. (6) and data in Figs. 2 and 3, the open-circuit voltage V_{oc} can be estimated for ICDs, ICD_SLs and QCDs under light illumination at an incident power density P_{inc}. Assuming P_{inc}=1 W/cm^2, about ten times that of the solar radiation at the surface of the earth, and the radiation source emits at the peak response wavelength (with spectral control in a TPV system) for ICDs and QCDs so that $J_{ph}=R_i \cdot P_{inc}$, V_{oc} is estimated and plotted in Fig. 4 for the devices shown in Fig. 3. As can be seen, QCDs have a very low V_{oc} (<3 mV) due to a high J_0 even with many stages (≥30), which may explain why QC PV cells have not been demonstrated in experiment. In contrast, the value of V_{oc} is significantly higher (more than an order of magnitude in most cases) for ICDs than for QCDs, which mainly results from the much lower J_0 in ICDs compared to QCDs (Fig. 2). Combined with the higher photocurrent density as implied in Fig. 3 (a), the IC structure is more advantageous than the QC structure for TPV applications. Note that, despite the much higher R_i (Fig. 3 (a)), V_{oc} is similar between ICD_SLs and ICDs because of the higher J_0 in ICD_SLs. However, with higher R_i and J_{ph}, ICD_SLs will have a higher output power and conversion efficiency when they have the same number of cascade stages.

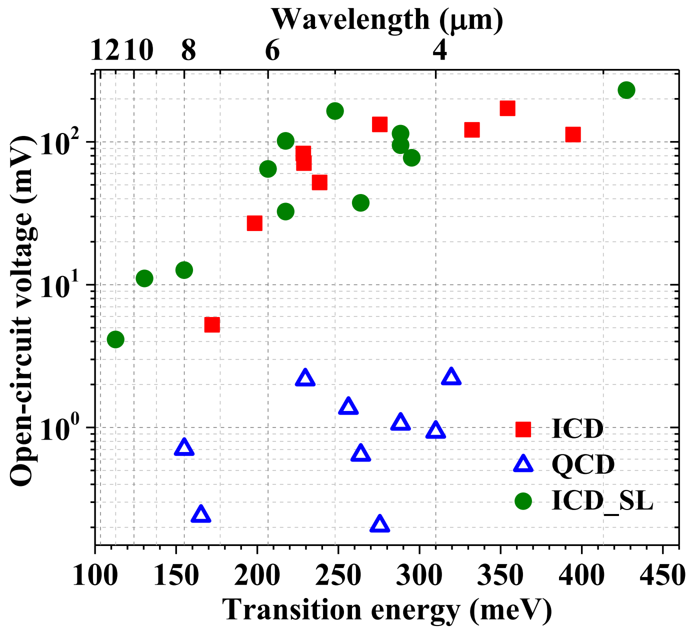

Fig. 4. Estimated V_{oc} at 300 K for the ICDs, ICD_SLs and QCDs shown in Fig.3.

6. Concluding Remarks

In summary, the saturation current density J_0 has been shown to reflect the fundamental difference in carrier lifetime between ICDs and QCDs. By analyzing and comparing available ICD and QCD data, we demonstrated that J_0 can be used as a unified figure of merit to evaluate both interband and intersubband cascade configurations in terms of their device functionality. The significance of J_0 on the detector and PV cell performances was illustrated by comparing the measured detectivity and the estimated open-circuit voltage, respectively. From extracted values of J_0, which were more than one order of magnitude lower in ICDs than in QCDs with similar transition energies, and discussion of the consequences on device performance, the advantages of interband cascade configurations over intersubband quantum cascade configurations were clearly revealed based on the same framework. The overall picture for both QCDs and ICDs sheds light from the perspective of a united figure of merit, which will provide useful guidance and stimulation to the future development of both ICDs and QCDs. It should be remarked that ICDs and QCDs both have their respective merits. For example, QCDs are narrow band devices based on more mature material systems with well-established epitaxial growth and device processing technologies. Consequently, at the present stage, QCDs can have better uniformity, less surface leakage, and higher output power as lasers (for applications where a high operating current density can be afforded with good thermal management). Hence, both QCDs and ICDs will coexist for various applications with different requirements.

Acknowledgments

We thank H. Ye and J. Gupta for the growth of some ICD wafers, Y. Li for measuring emission spectra of some ICLs, D. Hofstetter, J. Liu, K. Fujita, B. Schwarz, Q. K. Yang, T. Dougakiuchi and G. Strasser for providing help and data for QCDs. This work was supported in part by NSF (DMR-1608224 for TPV research and IIP-1640576 for laser research) and AFOSR (FA9550-15-1-0067 for ICIPs).

References

1. R. Q. Yang, "Infrared laser based on intersubband transitions in quantum wells," *Superlattices and Microstructures* **17**, 77 (1995).
2. R. Q. Yang, Chap. 12 in *Semiconductor lasers: fundamentals and applications*, edited by A. Baranov and E. Tournie (Woodhead Publishing Limited, Cambridge, UK, 2013).
3. I. Vurgaftman, R. Weih, M. Kamp, J.R. Meyer, C.L. Canedy, C.S. Kim, M. Kim, W.W. Bewley, C.D. Merritt, J. Abell, and S. Höfling, "Interband cascade lasers," *J. Phys. D. Appl. Phys.* **48**, 123001 (2015).
4. I. Vurgaftman, W. W. Bewley, C. D. Merritt, C. L. Canedy, M. V. Warren, C. S. Kim and J. R. Meyer, P. Geiser, M. Kim, "Sensitive Chemical Detection with Distributed Feedback Interband Cascade Lasers", in *Encyclopedia of Analytical Chemistry*, DOI: 10.1002/9780470027318.a9559 (John Wiley & Sons, Ltd. 2016).
5. J. V. Li, R. Q. Yang, C. J. Hill, and S. L. Chuang, "Interband cascade detectors with room temperature photovoltaic operation," *Appl. Phys. Lett.* **86** (10), 101102 (2005).
6. R. Q. Yang, Z. Tian, Z. Cai, J. F. Klem, M. B. Johnson, and H. C. Liu, "Interband-cascade infrared photodetectors with superlattice absorbers," *J. Appl. Phys.* **107** (5), 054514 (2010).
7. R. Q. Yang, Z. Tian, J. F. Klem, T. D. Mishima, M. B. Santos and M. B. Johnson, "Interband cascade photovoltaic devices," *Appl. Phys. Lett.* **96**, 063504 (2010).
8. H. Lotfi, R. T. Hinkey, L. Li, R. Q. Yang, J. F. Klem, and M. B. Johnson, "Narrow-Bandgap Photovoltaic Devices Operating at Room Temperature and Above with High Open-Circuit Voltage," Appl. Phys. Lett, **102**, 211103 (2013).
9. J. Faist, F. Capasso, D. L. Sivco, C. Sirtori, A. L. Hutchinson and A. Y. Cho, "Quantum Cascade Laser," *Science* **264**, 553 (1994).
10. M. Razeghi, N. Bandyopadhyay, Y. Bai, Q. Lu, and S. Slivken, "Recent advances in mid infrared (3-5μm) Quantum Cascade Lasers," *Optical Materials Express* **3**, 1872 (2013).
11. M. Troccoli, A. Lyakh, J. Fan, X. Wang, R. Maulini, A. G. Tsekoun, R. Go, and C. K. N. Patel, "Long-Wave IR Quantum Cascade Lasers for emission in the λ = 8-12 μm spectral region," *Optical Materials Express* **3**, 1546 (2013).
12. D. Hofstetter, M. Beck, and J. Faist, "Quantum-cascade laser structures as photodetectors," *Appl. Phys. Lett.* **81**, 2683 (2002).
13. F. R. Giorgetta, E. Baumann, M. Graf, Q. Yang, C. Manz, K. Köhler, H. E. Beere, D. A. Ritchie, E. Linfield, A. G. Davies, et al., "Quantum Cascade Detectors," *IEEE J. Quantum Electron.* **45**, 1039 (2009).
14. J. Yin, and R. Paiella, "Multiple-junction quantum cascade photodetectors for thermophotovoltaic energy conversion," *Opt. Express*. **18**, 1618 (2010).
15. J. Yin, and R. Paiella, "Limiting performance analysis of cascaded interband/intersubband thermophotovoltaic devices," *Appl. Phys. Lett*. **98**, 041103 (2011).
16. S.-Q. Zhai, J.-Q. Liu, K. Ning, F.-Q. L, L. Li, L.-J. Wang and Z.-G. Wang, "Strin-composed InP-based InGaAs/InAsAs Quantum Cascade Infrared Detectors for 3~5 μm Atmospheric Window," *Proc. SPIE* **8193**, 81931X (2011).
17. P. Reininger, B. Schwarz, H. Detz, D. MacFarland, T. Zederbauer, A. M. Andrews, W. Schrenk, O. Baumgartner, H. Kosina and G. Strasser, "Diagonal-transition quantum cascade detector," *Appl. Phys. Lett*. **105**, 091108 (2014).
18. X. Wang, J. Liu, S. Zhai, F. Liu, and Z. Wang, "Room temperature quantum cascade detector operating at 4.3 μm," *J. Semicond.* **35,** 104009 (2014).
19. P. Reininger, T. Zederbauer, B. Schwarz, H. Detz, D. MacFarland, A. M. Andrews, W. Schrenk, and G. Strasser, "InAs/AlAsSb based quantum cascade detector," *Appl. Phys. Lett*. **107**, 081107 (2015).
20. T. Dougakiuchi, K. Fujita, T. Hirohata, A. Ito, M. Hitaka and T. Edamura, "High photoresponse in room temperature quantum cascade detector based on coupled quantum well design," *Appl. Phys. Lett*. **109**, 261107 (2016); Erratum, **110**, 109902 (2017).

21. R. Q. Yang, C. J. Hill, L. E. Christensen, C. R. Webster, “Mid-IR type-II interband cascade lasers and their applications,” *Proc. SPIE*. **5624**, 413 (2005).
22. R. Q. Yang, L. Li, L. Zhao, Y. Jiang, Z. Tian, H. Ye, R. T. Hinkey, C. Niu, T. D. Mishima, M. B. Santos, et al., “Recent progress in development of InAs-based interband cascade lasers,” *Proc. SPIE.* **8640**, 86400Q (2013).
23. Y. Jiang, L. Li, R. Q. Yang, J. A. Gupta, G. C. Aers, E. Dupont, J. Baribeau, X. Wu and M. B. Johnson, “Type-I interband cascade lasers near 3.2 μm,” *Appl. Phys. Lett.* **106**, 041117 (2015).
24. S. M. S. Rassel, L. Li, Y. Li, R. Q. Yang, J. A. Gupta, X. Wu and G. C. Aers, “High-temperature and low-threshold interband cascade lasers at wavelengths longer than 6 μm,” *Opt. Eng.* **57** (1), 011021 (2018).
25. Y. Li, L. Li, W. Huang, R. Q. Yang, J. A. Gupta, X. Wu and G. C. Aers, “Low-threshold InAs-based interband cascade lasers near 6.3 μm,” In the abstract book of the 14th International Conference on Mid-IR Optoelectronics: Materials and Devices MIOMD-XIV at Flagstaff, AZ, USA (2018).
26. J. R. Meyer, C. A. Hoffman, F. J. Bartoli, and L. R. Ram-Mohan, “Type-II quantum-well lasers for the mid-wavelength infrared,” *Appl. Phys. Lett*. **67**, 757 (1995).
27. L. Lei, L. Li, H. Lotfi, H. Ye, R. Q. Yang, T. D. Mishima, M. B. Santos, and M. B. Johnson, “Midwavelength interband cascade infrared photodetectors with superlattice absorbers and gain,” *Opt. Eng.* **57** (1), 011006 (2018).
28. N. Gautam, S. Myers, A. V. Barve, B. Klein, E. P. Smith, D. R. Rhiger, L. R. Dawson, and S. Krishna, “High operating temperature interband cascade midwave infrared detector based on type-II InAs/GaSb strained layer superlattice*,” Appl. Phys. Lett.* **101**(2), 021106 (2012).
29. Z. Tian, R.T. Hinkey, R.Q. Yang, D. Lubyshev, Y. Qiu, J.M. Fastenau, W.K. Liu, and M.B. Johnson, "Interband cascade infrared photodetectors with enhanced electron barriers and p-type superlattice absorbers," *J. Appl. Phys*. **111** (2), 024510 (2012).
30. Z.-B. Tian, T. Schuler-Sandy, and S. Krishna, “Electron barrier study of mid-wave infrared interband cascade photodetectors,” *Appl. Phys. Lett.* **103**, 083501 (2013).
31. H. Lotfi, L. Lei, L. Li, R. Q. Yang, J. C. Keay, M. B. Johnson, Y. Qiu, D. Lubyshev, J. M. Fastenau and A.W.K. Liu, “High-temperature operation of interband cascade infrared photodetectors with cutoff wavelength near 8 μm”, *Opt. Eng.* **54** (6), 063103 (2015).
32. H. Lotfi, L. Li, L. Lei, Y. Jiang, R.Q. Yang, J.F. Klem, and M.B. Johnson, "Short-wavelength interband cascade infrared photodetectors operating above room temperature", *J. Appl. Phys*. **119** (2), 023105 (2016).
33. W. Huang, L. Lei, L. Li, J. A. Massengale, R. Q. Yang, T. D. Mishima, and M. B. Santos, “Current-matching versus non-current-matching in long wavelength interband cascade infrared photodetectors,” *J. Appl. Phys.***122**, 083102 (2017).
34. W. Huang, L. Lei, L. Li, J. A. Massengale, R. Q. Yang, T. D. Mishima and M. B. Santos, “Enhanced collection efficiencies and performance of interband cascade structures for narrow bandgap semiconductor thermophotovoltaic devices,” *J. Appl. Phys.* **124**, 023101 (2018).
35. R. T. Hinkey and R. Q. Yang, “Theory of Multiple-Stage Interband Photovoltaic Devices and Ultimate Performance Limit Comparison of Multiple-Stage and Single-Stage Interband Infrared Detectors”, *J. Appl. Phys.* **114**, 104506 (2013).
36. C. Koeniguer, G. Dubois, A. Gomez and V. Berger, “Electronic trnasport in quantum cascade strucutures at equilibrium,” *Phys. Rev. B*. **74**, 235325 (2006).
37. A. Buffaz, A. Gomez, M. Carras, L. Doyennette and V. Berger, “Role of subband occupancy on electronic transport in quantum cascade detectors,” *Phys. Rev. B*. **81**, 075304 (2010).
38. A. Delga, L. Doyennette, M. Carras, V. Trinite, and P. Bois, “Johnson and shot noises in intersubband detectors,” *Appl. Phys. Lett.* **102**, 163507 (2013).
39. W. Huang, L. Li, L. Lei, J. A. Massengale, H. Ye, R. Q. Yang, T. D. Mishima, M. B. Santos, “Minority carrier lifetime in mid-wavelength interband cascade infrared photodetectors,” *Appl. Phys. Lett.* **112** (25), 251107 (2018).

40. H. Schneider, and H. C. Liu, *Quantum Well Infrared Photodetectors* (Springer, 2007).
41. R. Q. Yang, J. M. Xu, and M. Sweeny, "Selection rules of intersubband transitions in conduction band quantum wells," *Phys. Rev. B* **50**, 7474 (1994).
42. D. Palaferri, Y. Todorov, A. Bigioli, A. Mottaghizadeh, D. Gacemi, A. Calabrese, A. Vasanelli, L. Li, A. G. Davies, E. H. Linfield, et al., "Room-temperature nine-μm-wavelength photodetctors and GHz-frequency heterodyne receivers," *Nature* **556**, 85-88 (2018).
43. W. Huang, L. Li, L. Lei, J. A. Massengale, R. Q. Yang, T. D. Mishima, M. B. Santos, "Electrical gain in interband cascade infrared photodetectors," *J. Appl. Phys.* **123**, 113104 (2018).
44. L. Lei, L. Li, H. Ye, H. Lotfi, R. Q. Yang, M. B. Johnson, J. A. Massengale, T. D. Mishima and M. B. Santos, "Long wavelength interband cascade infrared photodetectors operating at high temperatures," *J. Appl. Phys.* **120**, 193102 (2016).
45. A. Rogalski, *Infrared detectors*, second edition (CRC Press, Taylor & Francis Group, FL, US, 2011)
46. W. Shockley and H. Queisser, "Detailed balance limit of efficiency of *p-n* junction solar cells," *J. Appl. Phys.* **32**, 510 (1961).
47. T. Bauer, *Thermophotovoltaics: Basic Principles and Critical Aspects of System Design* (Springer, Berlin, Germany, 2011).
48. R. T. Hinkey, R. Q. Yang, "Theoretical Comparison of Performance Limits of Single- and Multiple-Stage Photovoltaic Devices," *Semicond. Sci. Technol.* **30**, 015013 (2015).
49. H. Lotfi, L. Li, L. Lei, R. Q. Yang, J. F. Klem, and M. B. Johnson, "Narrow-bandgap interband cascade thermophotovoltaic cells," *IEEE J. Photovoltaics* **7**, 146 (2017).